Electrolytic actuators: Alternative, high-performance, material-based devices

Colin G. Cameron and Michael S. Freund*

Molecular Materials Research Center, Beckman Institute M/C 139-74, California Institute of Technology, Pasadena, CA 91125

Communicated by Fred C. Anson, California Institute of Technology, Pasadena, CA, April 9, 2002 (received for review February 11, 2002)

The emerging field of materials-based actuation continues to be the focus of considerable research because of its inherent scalability and its promise to drive micromechanical devices that cannot be realized with conventional mechanical actuator strategies. The electrolytic phase transformation actuator offers a new broad-spectrum solution to the problem of direct conversion of electrical to mechanical energy. Strains of 136,000% and unoptimized work cycle efficiencies near 50% are demonstrated in a prototype device. Conceivably capable of generating stress beyond 200 MPa, this new approach promises performance orders of magnitude beyond other novel actuation strategies.

Recently there has been considerable interest in the development of materials to convert electrical energy directly to mechanical energy, and a number of new actuating materials are being developed to this end. These include electrochemically responsive conducting polymers (1, 2), capacitance-driven carbon nanotube actuators (3), pH-responsive hydrogels (4), ionic polymer metal composites (5), electric field responsive elastomers (6), and field electrostrictive polymers (7). The impetus behind this development is the need to create more efficient transduction that can be scaled to size or weight demands that cannot be fulfilled by conventional electric motors, pumps, and switches. These constraints are particularly relevant to the emerging fields of microfluidics, microelectromechanical systems, and robotics. Although many of the new materials under investigation exhibit useful specific properties, e.g., large stresses, sizable strains, or fast cycling time, they commonly suffer from inherent limitations that severely restrict their general applicability.

Although a significant amount of work has been directed toward developing new materials for actuation and pumping, the use of established, scalable electrochemical phase transformations has been largely overlooked. Although faradaic and nonfaradaic processes that lead to swelling and/or conformational changes within a material constitute an interesting approach to simple actuators (1–5), there are considerable advantages to pursuing processes that result in reversible phase transitions, particularly between liquid and gas. The greatest benefit of this particular transformation is the enormous volume and pressure changes that are obtainable. There are a few examples in the literature of electrolysis being used as the basis for microvalves (8), switches (9), dispensing systems (10), and dosing systems (11). However, these reports focus on the design of highly specialized microelectromechanical systems prototypes and do not explore the nature of the electrochemical reactions or their implications on design and performance of actuators in general. Consequently, they do not indicate the tremendous potential of this strategy relative to current state-of-the-art approaches to actuation. In this article a functioning electrolytic phase transformation (EPT) actuator prototype is introduced. Aspects of its performance are described, and its advantages over existing materials-based actuators are demonstrated.

The electrolysis of water (12, 13) to hydrogen and oxygen is perhaps the oldest example of direct conversion of electrical energy to pressure-volume changes. The reverse reaction, which is used in a fuel cell (14), converts the gas back to liquid. When the half-reactions are separated in a fuel cell, the rate of recombination is controlled via the external circuit, and the pressure-volume change can be converted back into electrical energy. Regenerative fuel cells (15) combine these two functions into one unit, and these devices are already finding applications where rechargeable, high-energy density devices are needed. Regenerative fuel cell systems have been demonstrated to have up to ≈70% electrical-to-electrical cycle efficiency for the H_2/O_2 cycle,[†] and cells based on other half-reactions are being explored for even higher efficiencies and current densities.

The two electrochemical half-reactions for the electrolysis of water are shown in Eqs. **1** and **2**. The net reaction (Eq. **3**) entails a 3:2 stoichiometric ratio of gas to liquid and occurs via the transfer of four equivalents of electrons through an external circuit.

$$2H_2O(l) \underset{\text{recombination}}{\overset{\text{electrolysis}}{\rightleftharpoons}} O_2(g) + 4H^+(aq) + 4e^- \quad [1]$$

$$4H^+(aq) + 4e^- \underset{\text{recombination}}{\overset{\text{electrolysis}}{\rightleftharpoons}} 2H_2(g) \quad [2]$$

$$\text{Net: } 2H_2O(l) \underset{\text{recombination}}{\overset{\text{electrolysis}}{\rightleftharpoons}} O_2(g) + 2H_2(g). \quad [3]$$

Since an actuator device based on these reactions is powered by the gas it generates, its response will be governed approximately by the ideal gas law:

$$PV = nRT. \quad [4]$$

The relationship provides two limiting scenarios.

Expansion Under Isobaric Conditions. This scenario represents the maximum fractional change in length $\Delta L/L$, or strain, that can be achieved in the form of linear displacement of a piston as the volume of the system grows. The charge passed during electrolysis and the reaction stoichiometry determine the volume of gas produced. The maximum strain that can be achieved with a piston driven by this process is a function of the volume of gas produced (Eq. **4**) and the volume of water consumed (Eq. **5**). At constant pressure,

$$V_{\text{gas}} = (3/2)n_{H_2O}RT/P \quad [5]$$

$$V_{\text{liquid}} = n_{H_2O} \times M_{H_2O}/\rho_{H_2O}, \quad [6]$$

where $M_{H_2}O$ and $\rho_{H_2}O$ are the molecular weight and density of water, respectively, and $n_{H_2}O$ moles of water are transformed. The maximum relative strain under ambient conditions can be calculated:

Abbreviations: EPT, electrolytic phase transformation; PEM, proton exchange membrane.

*To whom reprint requests should be sent at the present address: Department of Chemistry, University of Manitoba, Winnipeg, MB, Canada R3T 2N2. E-mail: michael_freund@umanitoba.ca.

[†]Molter, T., U.S. Department of Energy 1999 Review Conference on Fuel Cell Technology, August 3–5, 1999, Chicago.

CHEMISTRY

Table 1. Comparison of the performance of various actuation strategies

Actuator material	Maximum strain, %	Maximum pressure, MPa	Efficiency, %
Human skeletal muscle	>40*	0.35*	>35
Conducting polymers: (2)			
Drawn polyacetylene	0.45	450	
Undrawn polythiophene	1.1	37	
Field-actuated acrylic elastomer (6)	215*	2.4	90
Electromagnetic (voice coil)	50	0.1	90
Ceramic piezoelectric (16)	0.2*	110	90
Carbon nanotubes (3)	0.9*	0.75*	
Ionic polymer metal composite (17)	>10*	10–30*	
H_2–O_2 EPT	136,000*	200	70*

Information was taken from ref. 18 unless otherwise indicated.
*Experimentally measured values.

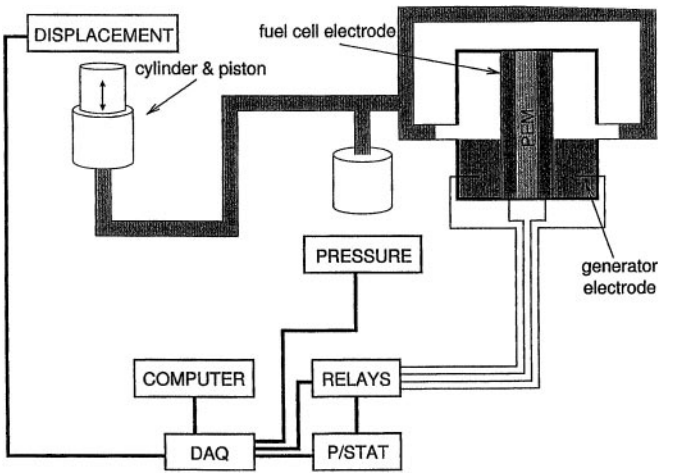

Fig. 1. Schematic of EPT actuator prototype, based on a regenerative fuel cell. DAQ, data acquisition; P/STAT, potentiostat.

$$\text{strain} = \frac{(\text{actuated length}) - (\text{unactuated length})}{(\text{unactuated length})} \quad [7]$$

$$= \frac{V_{\text{gas}} - V_{\text{liquid}}}{V_{\text{liquid}}} \quad [8]$$

$$\simeq \frac{V_{\text{gas}}}{V_{\text{liquid}}} \quad [9]$$

$$= \frac{(3/2)RT/P_{\text{atm}}}{M_{\text{H}_2\text{O}}/\rho_{\text{H}_2\text{O}}} \simeq 136{,}000\%. \quad [10]$$

Pressurization at Constant Volume. The buildup of pressure within the system by electrolysis represents the maximum force per cross-sectional area, or stress, that can be generated and applied through a piston. In the absence of piston motion (and flex in the system components), the maximum stress is reached when the gas is confined to the small volume made available by the water consumed (see Eq. **6**):

$$P = \frac{(3/2)n_{\text{H}_2\text{O}}RT}{V_{\text{liquid}}} \quad [11]$$

$$= \frac{(3/2)RT}{M_{\text{H}_2\text{O}}/\rho_{\text{H}_2\text{O}}} \simeq 200 \text{ MPa}. \quad [12]$$

These performance expectations are compared with other actuation strategies in Table 1. It is clear that EPT offers orders of magnitude better performance and with fewer design limitations. For example, materials that involve internal charging (e.g., carbon nanotubes, conducting polymers, and ionic polymer composites) require counterion flux through the material. Therefore these materials can be used efficiently only in the form of thin films, which limits the real distance over which they may operate. The common approach to achieving actuation in such thin film materials involves unimorph and bimorph configurations. This construct involves the coating of the active material on one or both sides of a flexible support. The stimulus response produces miniscule volume changes in the active material, and these are in turn amplified along the length of the support into a macroscopic bending motion. Several interesting devices based on conducting polymer active layers have exploited this flapping motion, and these include movable electrochromic pixels (19) and micromanipulators (20). However, despite large theoretical estimates of the stress of an expanding conducting polymer matrix (see Table 1), this approach cannot generate large linear forces, restricting the bimorph design to very specialized tasks. Further problems arise from the need to immerse the assembly in electrolyte to provide a source of counterions, although recent microencapsulation schemes (21) might alleviate that problem. For an EPT actuator, the electrolyte solution itself is the active material, and large forces are produced with ease. Piezoelectric materials can produce large stresses in very fast cycles, although with vanishingly small strain, again limiting their general applicability for actuation. Furthermore, the very high operating voltages demanded by piezoelectrics and other electric field responsive materials require additional engineering for their operation, making their scaling to microstructures problematic. Water electrolysis on the other hand requires only a few volts and produces enormous relative strains. In these and other non-EPT actuator strategies, directing energy transduction to usable linear motion is not a simple matter. On the other hand, the EPT actuator requires only a simple piston or a deflecting membrane. Therefore, this type of system is ideally suited to tasks that require long, powerful linear strokes, in a manner similar to conventional hydraulics, and indeed the maximum theoretical pressure output of an EPT system surpasses the typical operational pressure (≈20–80 MPa) of most standard hydraulic applications (22). Furthermore, the power source and drive unit can be decoupled in an EPT actuator, as in a hydraulic system, permitting greater application flexibility.

Methodology

To illustrate the potential of the EPT actuator, we constructed a prototype device based on a small fuel cell. The advantage of this configuration is that the rate of the recombination stage is maximized through the use of high surface area catalyst-loaded electrodes. However, one minor drawback of using a protein exchange membrane (PEM) regenerative fuel cell design is the problem of fuel crossover (23), where dissolved gases pass from one side of the cell through the membrane and react spontaneously at the catalyst surface on the other side, without requiring electrons to pass through the external circuit. This process leads to a gradual uncontrolled loss of pressure and/or volume. Crossover can be compensated by a simple feedback mechanism where additional electrolysis is undertaken to negate its effects, which results in a slight loss of efficiency. The prototype is shown schematically in Fig. 1. Two 16-cm^2 platinum-impregnated carbon cloth electrodes (E-tek ECC 40% Pt on Vulcan XC-72, 2.0 $mg{\cdot}cm^{-2}$ Pt, E-tek, Somerset, NJ) were held against a Nafion 117

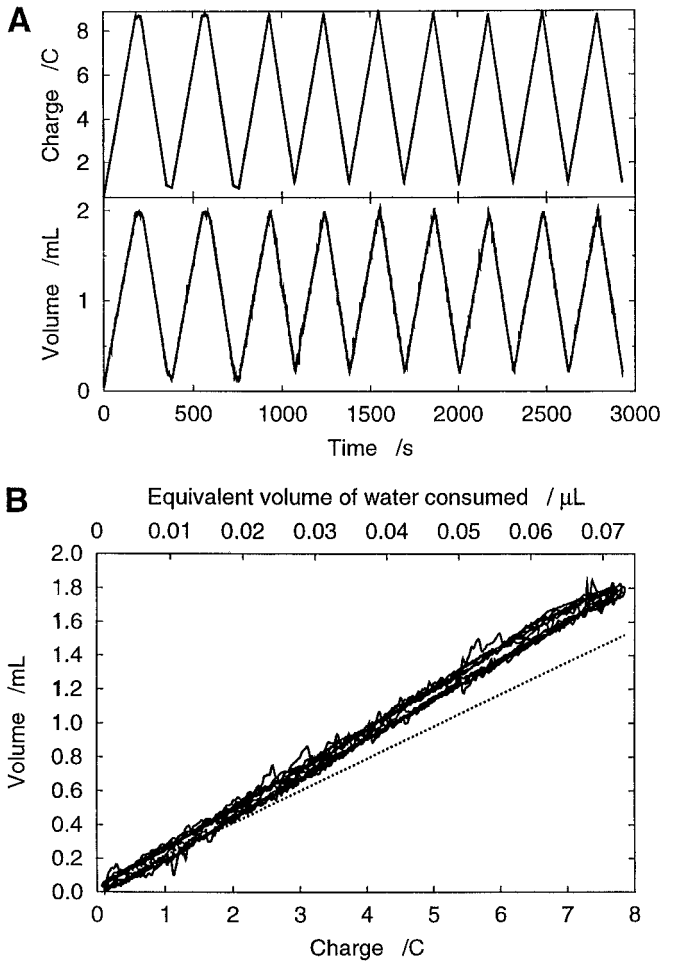

Fig. 2. (*A*) Charge and volume displacement profiles in an EPT system at constant pressure. Charge is corrected for a 3.7-mA crossover current. (*B*) Charge and volume correlation. The equivalent volume of water consumed, which is proportional to charge, is indicated. Predicted response (dotted line) is based on stoichiometry, the ideal gas law, and Faraday's law.

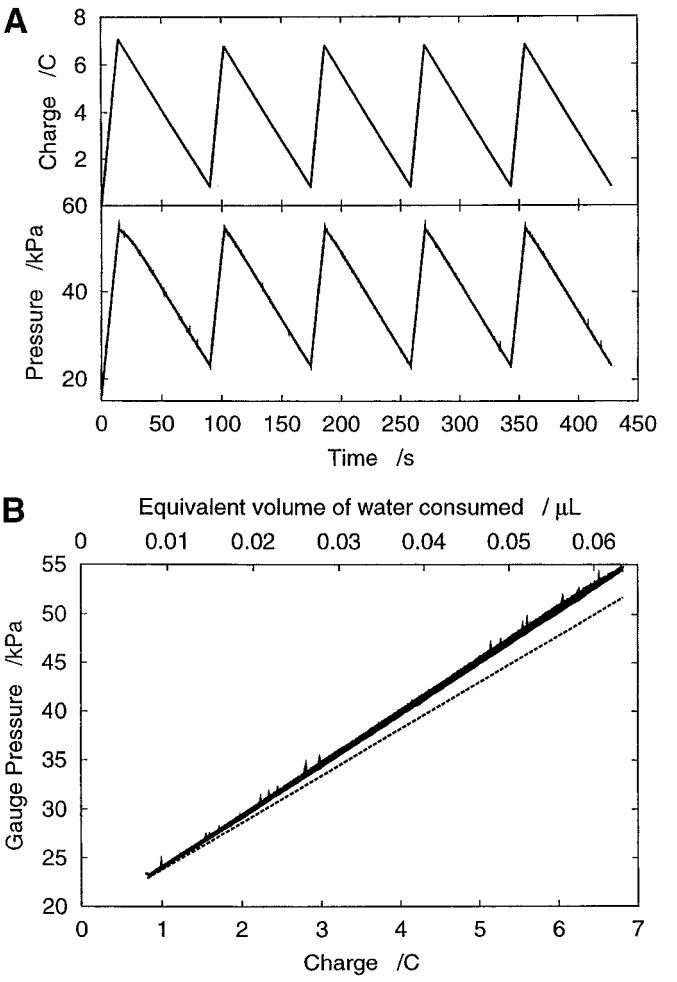

Fig. 3. (*A*) Charge and pressure profiles in an EPT system at constant volume. Charge is corrected for a 7.0-mA crossover current. (*B*) Charge and pressure correlation. The equivalent volume of water consumed, which is proportional to charge, is indicated. Predicted response (dotted line) is based on stoichiometry, the ideal gas law, and Faraday's law and assumes 4 ml of headspace gas.

PEM (0.007 inch thick, Aldrich) by perforated stainless-steel plates, which also provided an electrical contact. The membrane was pretreated (24) by boiling in 3% H_2O_2, then in water, 0.5 M H_2SO_4, and finally again in water, and stored in water until needed. Platinum wire or mesh generator electrodes were fitted, and the assembly was held in place and sealed with clear plastic plates, with the two compartments holding a volume of about 4 ml each. The cell and tubing were filled with 1.0 M H_2SO_4, which served as both the active material and hydraulic fluid. Both compartments operated in parallel through the use of a T junction in the tubing, ensuring no pressure difference between the compartments could develop. The fluid flow in the tubing was then directed either to a reservoir, for volume measurements, a SenSym (Milpitas, CA) 19U030PA4K transducer for pressure measurements, or a 3.6-cm^2 piston for work cycles. The cell was operated so that approximately half of the area of each carbon cloth fuel cell electrode was exposed to electrolytically generated gas. Mechanical relays were used to select either electrolysis or fuel cell electrode pairs and these, along with a potentiostat (EG & G model 362, Princeton Applied Research) and other related equipment, were controlled by custom software running under LINUX on a computer equipped with a National Instruments (Austin, TX) PCI-MIO-16XE data acquisition board and the libcomedi (maintained by David Schleef) interface library. Electrolysis was carried out under controlled current conditions, maintaining an operating voltage around 3 V, and pulsed to throttle expansion to preset rates. Unless stated otherwise, current was corrected for gas permeation through the Nafion PEM (23). This crossover current appeared as additional charge input needed to maintain the system at constant pressure or volume and was typically on the order of 0.5 $mA \cdot cm^{-2}$ of cell cross-sectional area exposed to gas.

Results

The prototype apparatus was used to demonstrate EPT performance in the two limiting cases of expansion at constant pressure and pressurization at constant volume. It also was used in a mechanical work cycle to examine the efficiency of an EPT actuator under typical working conditions.

Expansion. Volume displacement experiments under isobaric conditions were conducted by measuring the mass of fluid moving in or out of the cell and correcting for density. A typical volume profile is shown in Fig. 2*A*, where the system was run through a program of triangular cycles. The maximum (short circuit) volume retraction rate that could be achieved with the

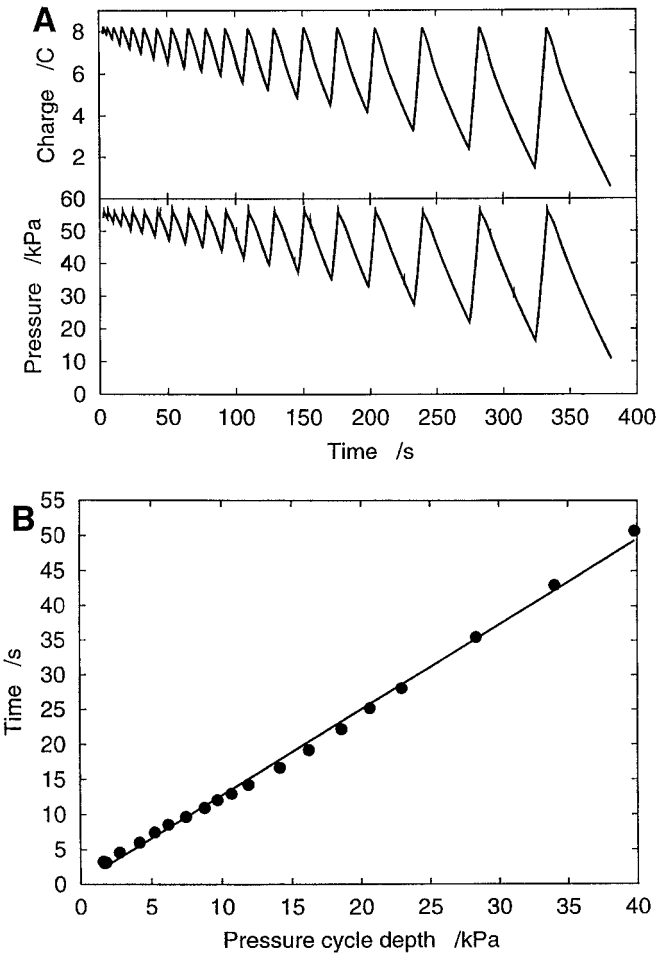

Fig. 4. (*A*) Charge and pressure profiles in an EPT system at constant volume and with a changing pressure range. Charge is corrected for a 5.7-mA crossover current. (*B*) Cycle period is linear with cycle depth.

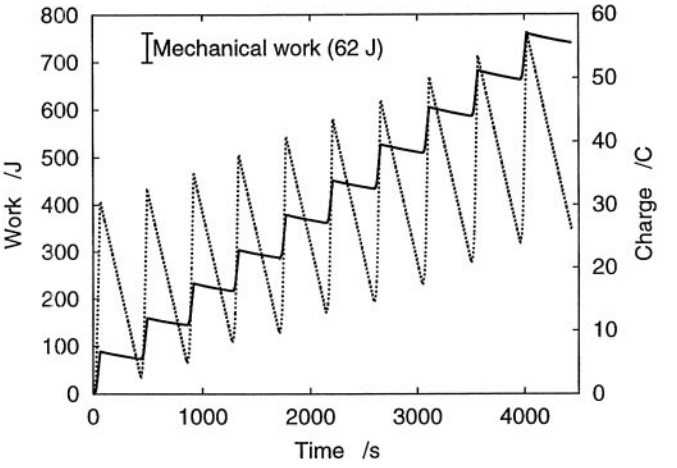

Fig. 5. Electrical work (solid line) (obtained by the integration of the product of current and potential over time) and uncorrected charge (dotted line) cycles for lifting a 1.26-kg load through a fixed distance (5 mm) by using a 3.6-cm^2 piston. The theoretical mechanical work for this process is indicated. No attempts were made to compensate for crossover, friction, heat dissipation, flex, or any other energy-consuming processes that lead to diminished efficiency.

electrodes used was 4 μl·s^{-1}·cm^{-2} of exposed electrode area.[‡] The effect of crossover appears in a plot of charge versus time as a small sloping background that can be subtracted. The data here have been corrected for crossover in this manner. Fig. 2*B* correlates expansion and charge, where a reproducible response profile ensues with expansion slightly greater than predicted from the stoichiometry, Faraday's law, and the ideal gas law. This deviation is possibly caused in part by additional expansion caused by resistive heating.[§] The good correlation with the predicted response indicates this system exhibited strain beyond 136,000%.

Pressurization. A typical pressure program is shown in Fig. 3, again with correction for crossover current. There is a good correlation with the predicted response that assumes a constant volume of gas. This volume was estimated based on the cell dimensions, and error in this value along with resistive heating could account for the small discrepancy between the anticipated and observed response. The system was subjected to a series of pressure cycles of changing amplitude, shown in Fig. 4*A*. The duration of a cycle is proportional to the cycle amplitude, as indicated in Fig. 4*B*. This result illustrates the capability of the EPT design to perform consistently under varying operational parameters, with the nature of the fuel cell electrode determining the rate of pressure drop and hence cycle time. The most rapid pressure drop that could be attained by this prototype was 1.4 kPa·s^{-1}·cm^{-2} at short circuit. The prototype reached a maximum cycle rate of 0.67 Hz for a 0.8-kPa oscillation. This artificial limit was imposed by the control software. This rate compares well with the most rapid conducting polymer bimorph actuators, and higher frequencies and amplitudes are expected in systems operating at higher temperature and pressure and with more optimized electrode materials and better cell design.

Work Cycle. The prototype actuator assembly was driven through work cycles by lifting and lowering a block of known mass through a known distance by using a piston in a 3.6-cm^2 bore. Electrical work, obtained by the integration of the product of current and potential over time, is plotted in Fig. 5 along with charge (not corrected for crossover) for the motion of a 1.26-kg weight through a vertical distance of 5 mm. The recombination was arbitrarily at a current density $j \simeq 5$ mA·cm^{-2}. The electrolysis-powered extension required an average input of 87 J, and 16 J was recouped during retraction, representing 71% and 26% efficiency, respectively, for the two halves of the cycle, giving a net 48% round-trip efficiency. Our values represent a lower limit on efficiency because no attempts were made to compensate for crossover, friction, heat dissipation, flex, or any other energy-consuming processes that lead to diminished efficiency. The effect of friction in the driven piston is shown in Fig. 6, where the slave piston was held nearly motionless while the device was driven through triangular pressure cycles. A hysteresis ensues as the force applied by the piston lags the input charge caused by the friction in the cylinder that must be first overcome. The frictional force of the piston in the cylinder can be measured independently and is approximately equal to the force corresponding to the charge (the relationship indicated in Fig. 3*B*) in the horizontal region of the hysteresis loop. However, despite such losses, the system still exhibits impressive overall efficiency.

The excellent performance of this unoptimized prototype underlines the enormous potential of the EPT actuation strat-

[‡]This refers to the cross-sectional area of the fuel cell cathode, and hence of the whole cell. Since O_2 reduction is the limiting process in a H_2/O_2 PEM fuel cell, the performance predictions that follow are also based on the area of exposed cathode.

[§]An expansion of 0.1 ml in a gas headspace of 4 ml would require a temperature increase of 7°C.

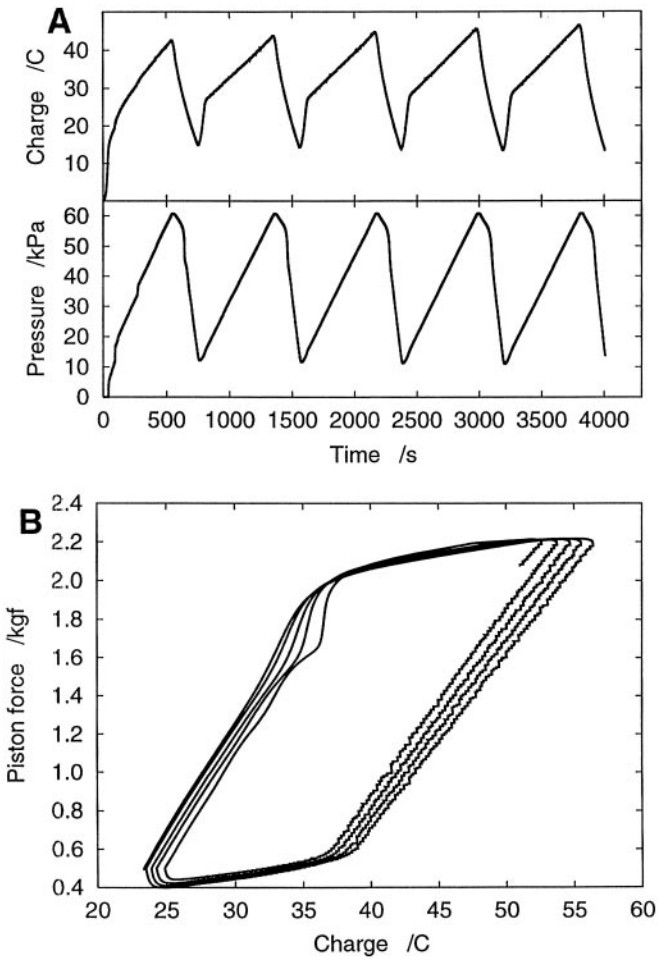

Fig. 6. (*A*) Charge and pressure profiles in an EPT system at constant volume. (*B*) Force output of a 3.6-cm^2 piston that was held motionless.

egy. We have shown that the device performs as anticipated, producing strains beyond 136,000%. Stress response was also in accordance with prediction, although the mechanical strength of the apparatus limited tests to 70 kPa. These enormous pressure-volume changes are directed in long, linear, powerful strokes. The primary shortcoming of materials-based actuation strategies to date is their inability to generate long linear power strokes at low voltages.[¶] The EPT actuator performs this function with ease, with a maximum theoretical stress that surpasses the typical operational pressure (≈20–80 MPa) of most standard hydraulic applications (22). Furthermore, the power source and drive unit can be decoupled in an EPT actuator, as in a hydraulic system, permitting even greater application flexibility.

The primary advantage that sets EPT actuation apart from other materials-based actuation strategies is that it is limited not by the active material—water—but only by the cell design, electrode properties, and operating parameters such as temperature and pressure. The rate of gas recombination limits the retraction portion of the work cycle. In our cell this process was limited to 4 $\mu l \cdot s^{-1} \cdot cm^{-2}$ and 1.4 $kPa \cdot s^{-1} \cdot cm^{-2}$ of exposed electrode area for volume and pressure, respectively. However, this aspect of the system can piggyback the ongoing steady improvements in PEM fuel cell technology. For example, the current density in state-of-the-art hydrogen fuel cells already surpasses 2.5 $A \cdot cm^{-2}$, a figure that would correspond to a volume retraction of 0.9 $ml \cdot s^{-1} \cdot cm^{-2}$ and a pressure drop of 370 $kPa \cdot s^{-1} \cdot cm^{-2}$ in our configuration. The underlying regenerative fuel cell technology is well established, and the materials are relatively inexpensive. The active material is low weight and nontoxic, and the cycle operates at low voltages and relatively high efficiency, with energy recovery available during the retraction stroke.

The advantages of the EPT actuator strategy are clear. Powerful linear actuation can be obtained from a scalable, efficient, lightweight, low-voltage device. This approach offers new solutions to perennial problems in many fields, ranging from microfluidics and microelectromechanical systems to mechanical engineering and space robotics.

[¶]Devices using potential-driven differential surface tension, or ''continuous electrowetting,'' to drive small plugs of fluid linearly along a capillary have been demonstrated (25). Since this effect stems entirely from induced changes in surface free energy and does not inflict any sort of physical change in the medium, it is not *per se* a materials-based actuation strategy.

This work was supported by the Arnold and Mabel Beckman Foundation.

1. Jager, E. W. H., Smela, E. & Inganäs, O. (2000) *Science* **290,** 1540–1545.
2. Baughman, R. H. (1996) *Synth. Met.* **78,** 339–353.
3. Baughman, R. H., Cui, C., Zakhidov, A. A., Iqbal, Z., Barisci, J. N., Spinks, G. M., Wallace, G. G., Mazzoldi, A., Rossi, D. D., Rinzler, A. G., *et al.* (1999) *Science* **284,** 1340–1344.
4. Shibayama, M. & Tanaka, T. (1993) *Adv. Polym. Sci.* **109,** 1–62.
5. Shahinpoor, M. & Kim, K. J. (2001) *Smart Mater. Struct.* **10,** 819–833.
6. Pelrine, R., Kornbluh, R., Pei, Q. & Joseph, J. (2000) *Science* **287,** 836–839.
7. Zhang, Q. M., Bharti, V. & Zhao, X. (1998) *Science* **280,** 2101–2104.
8. Neagu, C. R., Gardeniers, J. G. E., Elwenspoek, M. & Kelly, J. J. (1997) *Electrochim. Acta* **42,** 3367–3373.
9. Jackel, J. L., Johnson, J. J. & Tomlinson, W. (1990) *Opt. Lett.* **15,** 1470–1472.
10. Stanczyk, T., Ilic, B., Hesketh, P. J., James, G. & Boyd, I. (2000) *J. Micromech. Syst.* **9,** 314–320.
11. Böhm, S., Timmer, B., Olthuis, W. & Bergveld, P. (2000) *J. Micromech. Microeng.* **10,** 498–504.
12. Nicholson, W. (1800) *J. Nat. Philos. Chem. Arts* **4,** 179–187.
13. Faraday, M. (1834) *Philos. Trans.* **124,** 77–122.
14. Grove, W. (1839) *Philos. Mag. Ser. 3* **14,** 127–130.
15. Findl, E. & Klein, M. (1967) in *Regenerative EMF Cells* (Am. Chem. Soc., Washington, DC), pp. 292–305.
16. Park, S.-E. & Shrout, T. R. (1997) *J. Appl. Phys.* **82,** 1804–1811.
17. Shahinpoor, M., Bar-Cohen, Y., Xue, T., Simpson, J. & Smith, J. (1998) *Proc. SPIE 5th Annu. Int. Symp. Smart Struct. Mater.* **3324,** 251–267.
18. Kornbluh, R., Pelrine, R., Pei, Q., Oh, S. & Joseph, J. (2000) *Proc. SPIE Smart Mater.* **3987,** 51–64.
19. Smela, E. (1999) *Adv. Mater.* **11,** 1343–1345.
20. Jager, E. W. H., Inganäs, O. & Lundström, I. (2000) *Science* **288,** 2335–2338.
21. Madden, J. D., Cush, R. A., Kanigan, T. S. & Hunter, I. W. (2000) *Synth. Met.* **113,** 185–192.
22. Pinches, M. J. & Ashby, J. G. (1989) *Power Hydraulics* (Prentice–Hall, Englewood Cliffs, NJ).
23. Broka, K. & Ekdunge, P. (1997) *J. Appl. Electrochem.* **27,** 117–123.
24. Ticianelli, E., Deroin, C., Redondo, A. & Srinivasan, S. (1988) *J. Electrochem. Soc.* **135,** 2209–2217.
25. Lee, J. & Kim, C.-J. (2000) *J. Microelectromech. Syst.* **9,** 171–180.